



Design and development of high-performance metamaterial absorber for moisture-sensing application

Atipriya Sharma¹ · Harbinder Singh² · Amit Gupta³

Received: 14 November 2022 / Accepted: 20 April 2023 / Published online: 26 April 2023
© The Author(s), under exclusive licence to Springer-Verlag GmbH, DE part of Springer Nature 2023

Abstract

Metamaterials are frequently employed as sensors in a wide range of applications because of their special qualities that are not present in nature. This study focus on the design, fabrication and measurement of a novel shape metamaterial absorber for moisture-sensing applications. The proposed metamaterial absorber consists of modified cross along with split square resonator shape conductor on top of a 0.6 mm thick substrate. Parametric studies are also performed on the different design parameters, such as the thickness of the substrate and split square resonator etc. to figure out the optimal value of design variables. The simulated results of the proposed absorber illustrate the maximum reflection coefficient at 9.9 GHz. The obtained reflection coefficient value is -30.5 dB at the resonant frequency. The measured results of the absorber also show good agreement with the simulated results. Furthermore, the proposed metamaterial-based absorber utilize as a sensor. The proposed sensor design demonstrates excellent results in terms of resonance shift, sensitivity, linearity, Q factor, and figure of merit, making it a good candidate for moisture-sensing applications.

Keywords FoM · Metamaterial absorber · Moisture sensor · Sensitivity · X-band

1 Introduction

An electromagnetic wave's polarization, magnitude, and phase can all be controlled and altered using metamaterials (MM), which have extraordinary properties. The theory of Metamaterials has been commenced by Veselgo et al. [1] in 1968. Since, then this concept has been globally exploited by engineers and physicists for distinct applications like in antennas absorber [2] and sensors [3, 4]. MM are synthetic or man-made materials with unique characteristics like a negative index of refraction (n), negative permeability (μ) and permittivity (ϵ) [5]. The structure, volume, and arrangements of the unit cell provide the distinctive and valuable qualities of MM instead of the composition of the material

[6]. The traditional absorbers are expensive as they are bulky due to their high thickness which limits their application in today's era. Therefore, conventional absorbers are replaced by the MM-based absorbers; first, it was investigated by Landy et al. [7] in 2008. Numerous microwave absorption structures are proposed by authors and accessible in literature based on a single band, dual-band and broadband absorption on different frequencies [8–11]. The multi-layering structures are also proposed by the different authors in the literature to obtain the multiband and broadband absorption characteristics, but simultaneously it increases the cost of fabrication and complexity too [12]. Recently investigators are also attracted to the polarization insensitivity of the absorber with the utilization of resistors [13]. In spite of that, a cost-effective, low thickness, polarization-insensitive and single-layer absorber is still a difficult aspect among scholars. An author has demonstrated an MM-inspired wideband absorber of 8.30 GHz from 6.86 to 15.16 GHz [14]. Bakir et.al propounded an ultrathin MM-based absorber, which demonstrates wideband and narrowband behavior by selecting an FSS substrate and by determining the proper FSS shape [15].

To meet the requirements of the various applications, various MM absorbers with various absorption bandwidths

✉ Harbinder Singh
harvinder90@gmail.com

¹ Chitkara University Institute of Engineering and Technology, Chitkara University, Rajpura, Punjab, India

² Department of Electronics and Communication Engineering, Chandigarh University, Mohali, Punjab, India

³ Department of Electronics and Communication Engineering, I.K Gujral Punjab Technical University, Kapurthala, Punjab, India

have been proposed thus far. MM absorbers can be broadly categorized into two categories based on their absorbing bandwidths: narrow and wide. Applications for wideband spectra include photodetectors and solar energy harvesting [16]. Narrowband spectra, on the other hand, have possible applications in thermoelectric, sensors, and a variety of other fields. Moisture sensing is a key area of research for sensing technologies and has received a lot of attention. Water could be found in a wide range of environmental and fabricated products. Water content is commonly referred to as moisture content, and is widely used to assess product quality as well as ideal collection and storage requirements.

In this study, a novel ultra-thin narrow band MM absorber is analyzed and designed. The main innovation of the study is the high absorption efficiency and tunability of the metamaterial absorber. This is achieved using a double-layer structure consisting of a metallic metamaterial resonator film and ground plane, which allows for a high degree of control over the absorption properties of the structure. The proposed absorber is also attractive for practical applications due to its low-cost and scalable fabrication process. The metamaterial absorber has potential applications in energy harvesting, sensing, and stealth technology. The absorber is also tuned for moisture-sensing applications in the X band, demonstrating its potential for practical applications in various fields. The study is divided into three more sections. Section 2 details the design and analysis part of the proposed sensor. The moisture-sensing properties of the proposed MM absorber sensor is investigated in Sect. 3. The research is concluded in Sect. 4.

2 Design of MM-based structure

In this design, the MM unit cell is a single layer consisting of a split square resonator (SSR) with modified cross in between SSR. The backplane of the structure is completely covered by the metallic layer. The structure is etched on the 0.6 mm thick FR4 substrate whose dielectric constant is 3 and the loss tangent is 0.025. The absorption of the absorber can be expressed as $A(\omega) = (1 - R(\omega) - T(\omega))$, where $R(\omega)$ is the reflection and $T(\omega)$ is the transmission [17]. In this prototype, the structure is completely backed by a metallic thin film to restrict the transmission. Therefore, for this structure absorption is based on reflection only. The unit cell of the presented structure is illustrated in Fig. 1. Table 1 represents the values of the MM unit cell dimensions which are illustrated in Fig. 1. This structure is simulated in Computer Simulation Technology (CST) Microwave Studio. The structural dimensions of the MM-based unit cell are refined using mathematical models based on a frequency domain solver. The goal of the optimized procedure is to achieve the resonance in X-band with higher absorption. Initially, the

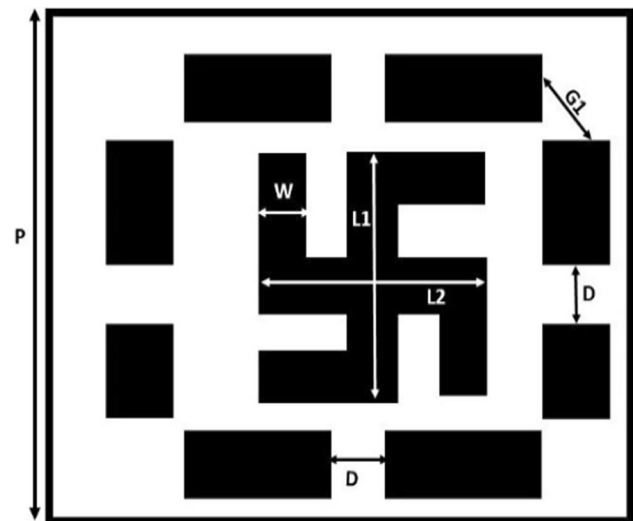


Fig. 1 Front view of the MM-based structure

Table 1 Optimized dimensions of the MM unit cell

Dimension	Value (mm)	Dimension	Value (mm)
P	9.5	L2	5
W	1	G1	1.1
L1	5	D	1

thickness of the FR4 substrate has been optimized to obtain the maximum absorption in the desired band. After determining the thickness of the substrate, the other parameters of the MM-based unit cell were optimized.

2.1 Simulated results

Figure 2 illustrates the reflection coefficient of the MM-based structure. It has been perceived that the peak of the resonance is at 9.9 GHz with a -30.5 dB value of the reflection coefficient. The surface current distribution of the structure is also studied and portrayed in Fig. 3. It has been noticed that at 9.9 GHz maximum absorption is due to modified cross resonator and corners of SSR. The narrow band response is observed with a FWHM (Full Width Half Maxima) bandwidth of 203 MHz from 9.86 to 10.0 GHz. Furthermore, parametric studies are performed to know the optimal value of substrate thickness and other parameters of the MM unit cell, as shown in Fig. 4a. The optimal value of the thickness of the dielectric substrate is 0.6 mm, as we can perceive that as the thickness of the substrate is increasing, the reflection coefficient graph is shifting below -10 dB. As the reflection is directly proportional to the thickness of the substrate. The peak resonance and highest maximum absorption are observed at 9.9 GHz with 0.6 mm thickness.

Fig. 2 Reflection coefficient of the MM-based structure

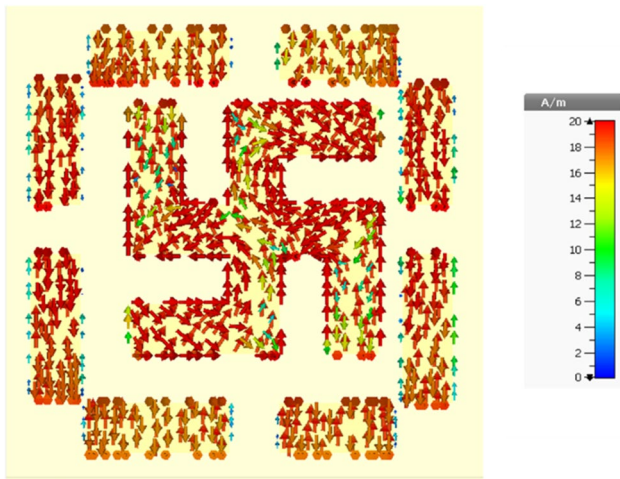
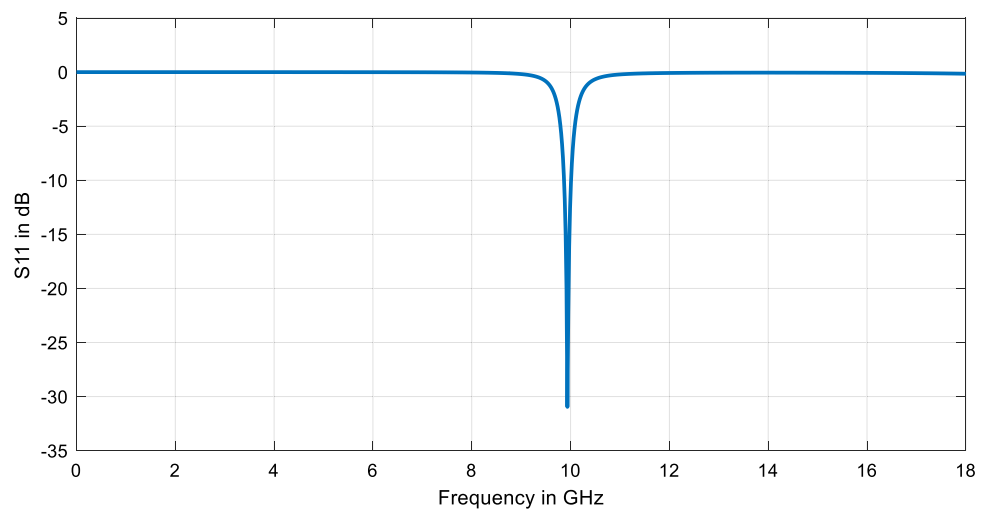


Fig. 3 Surface current distribution at 9.9 GHz

The second study is performed on the scaling of the modified cross resonator as this geometry plays a vital role in the absorption. The study of scaling has been performed from 0.2 to 1 range, as beyond that range the SSR and modified cross resonator get overlap each other. Figure 4b illustrates the performance of scaling in terms of reflection coefficient, and it has been observed that as the size of the modified cross resonator increases, the change in the value of inductance and capacitance resultant resonance shifts towards the lower frequency.

The prime requirement of the MM unit cell is single resonance with maximum absorption as further it will be utilized as a sensor. The next simulation is performed on the center slits of the SSR. Figure 4c depicts the variation in the gap of the square in terms of the reflection coefficient. It has been observed that at different values the reflection coefficient value is shifting towards 0 dB, with multiple resonances. The optimum value of the gap is 1.1 mm, where

the maximum absorption with single resonance is achieved. Meanwhile, one more study is performed on the edges of the SSR. The value of the edges varied from 1.0 to 1.8 mm with a 0.2 mm gap. At 1.6 mm and 1.8 mm multiple resonances have been observed with the shifting of resonance towards higher frequency. The best absorption is achieved at 1.4 mm; therefore, it has been considered as optimal value.

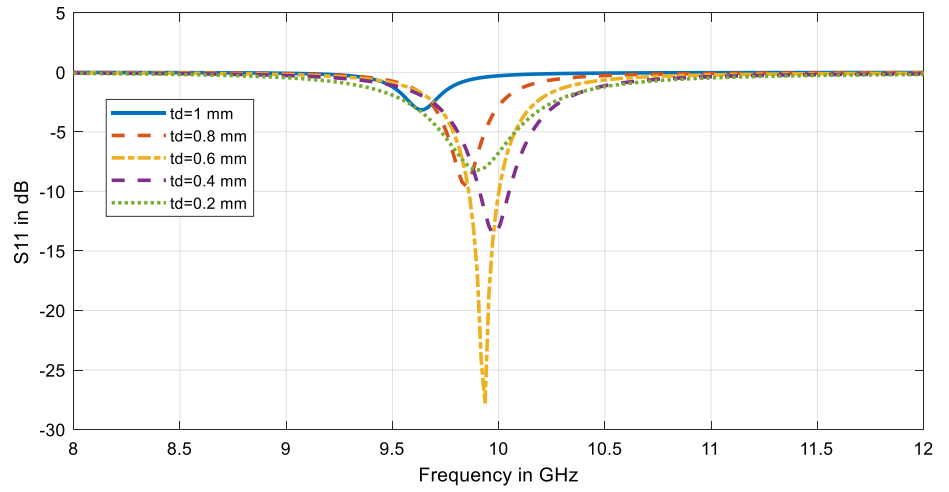
One step further, simulated reflection coefficient graphs of the proposed MM unit cell are illuminated in Fig. 5a for transverse magnetic (TM) and transverse electric (TE) polarization. Whereas, Fig. 5b shows the reflection coefficient graph for different polarization angles. Figure 5a shows the variations in the reflection coefficient graph at 9.9 GHz under TE polarization. As the angle increases from 0° to 60° the bandwidth gets reduced due to the shifting of the reflection coefficient towards 0 dB. Whereas, in TM polarization after 40° it shows similar behavior as TE polarization but below 40° not much variation has been observed. The proposed design is simulated from 0° to 60° under distinct polarization angles. It is observed from Fig. 5b that the prototype illuminates polarization-insensitive behavior as the MM-based absorber is a fourfold symmetrical design.

2.2 Fabrication and measurement

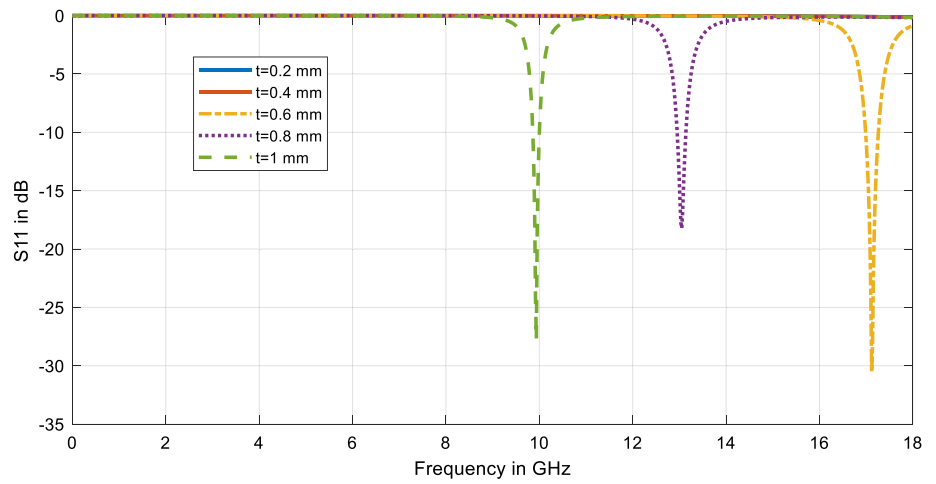
The final design of the metamaterial structure was exported from CST Microwave Studio and printed on a 0.6 mm thick FR4 substrate using standard PCB technology [18]. This process involves etching copper cladding from the FR4 substrate using a standard photolithography process, which includes several steps to ensure proper fabrication [19].

First, the FR4 substrate was cleaned thoroughly with acetone and isopropyl alcohol to remove any dust, dirt or contaminants that may have interfered with the fabrication process. A thin layer of copper cladding was then laminated to the FR4 substrate using a hot press. Next, a layer

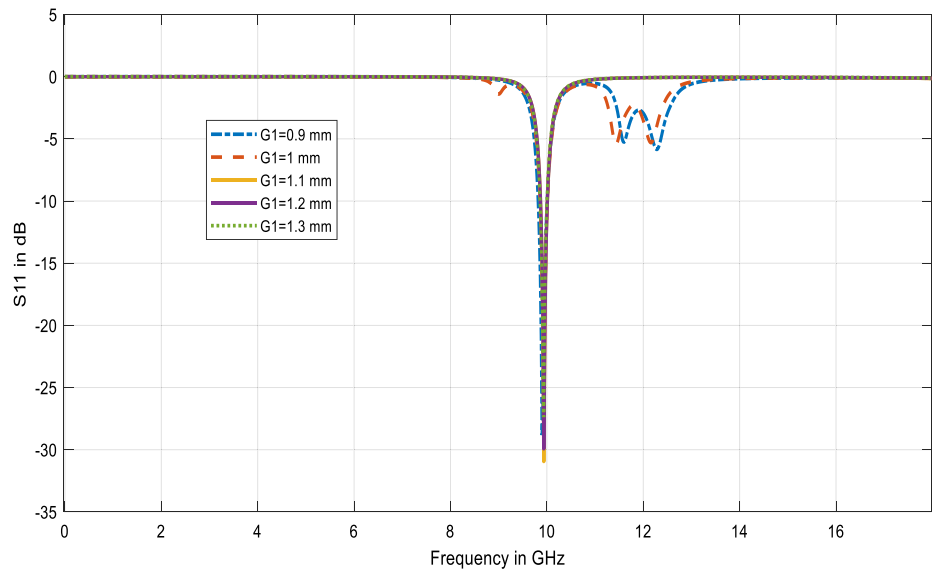
Fig. 4 Parametric study on **a** substrate thickness, **b** scaling of modified cross, **c** scaling of SSR and **d** gap between SSR



(a)

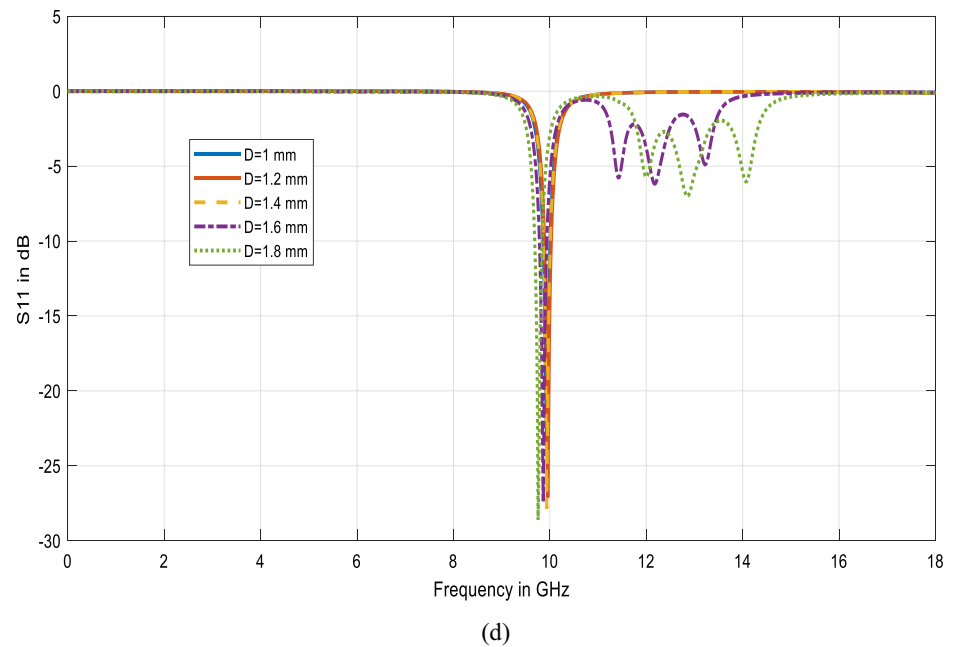


(b)



(c)

Fig. 4 (continued)



of photoresist was coated on the copper cladding and the photoresist was exposed to UV light using a mask aligner [20]. The exposed photoresist was then developed using a developer solution to remove the unexposed areas of the photoresist, leaving only the desired pattern.

The copper cladding was then etched using a ferric chloride solution to create the desired metamaterial structure. Finally, the remaining photoresist was stripped using a solvent to reveal the copper metamaterial structure. The sample was prepared as an array of the unit cell by considering the homogenous properties of the unit cell used in simulation [21]. The dimension of the fabricated structure was chosen to be $256 \times 256 \text{ mm}^2$ to avoid any edge diffraction. The front view of the fabricated prototype is demonstrated in Fig. 6a.

To investigate the performance of the fabricated metamaterial structure, it was subjected to a free-space microwave measurement setup in an anechoic chamber. This measurement setup was designed to analyze the reflection coefficient of the metamaterial absorber to determine its absorptive properties [22]. This setup included a broadband horn antenna and vector network analyzer (VNA) (Keysight E5063A) for measuring the reflection coefficient of the metamaterial absorber. The reflection coefficient was measured in the frequency range of 0–18 GHz under normal incidence to analyze the absorptive behavior of the metamaterial structure, as illustrated in Fig. 6b.

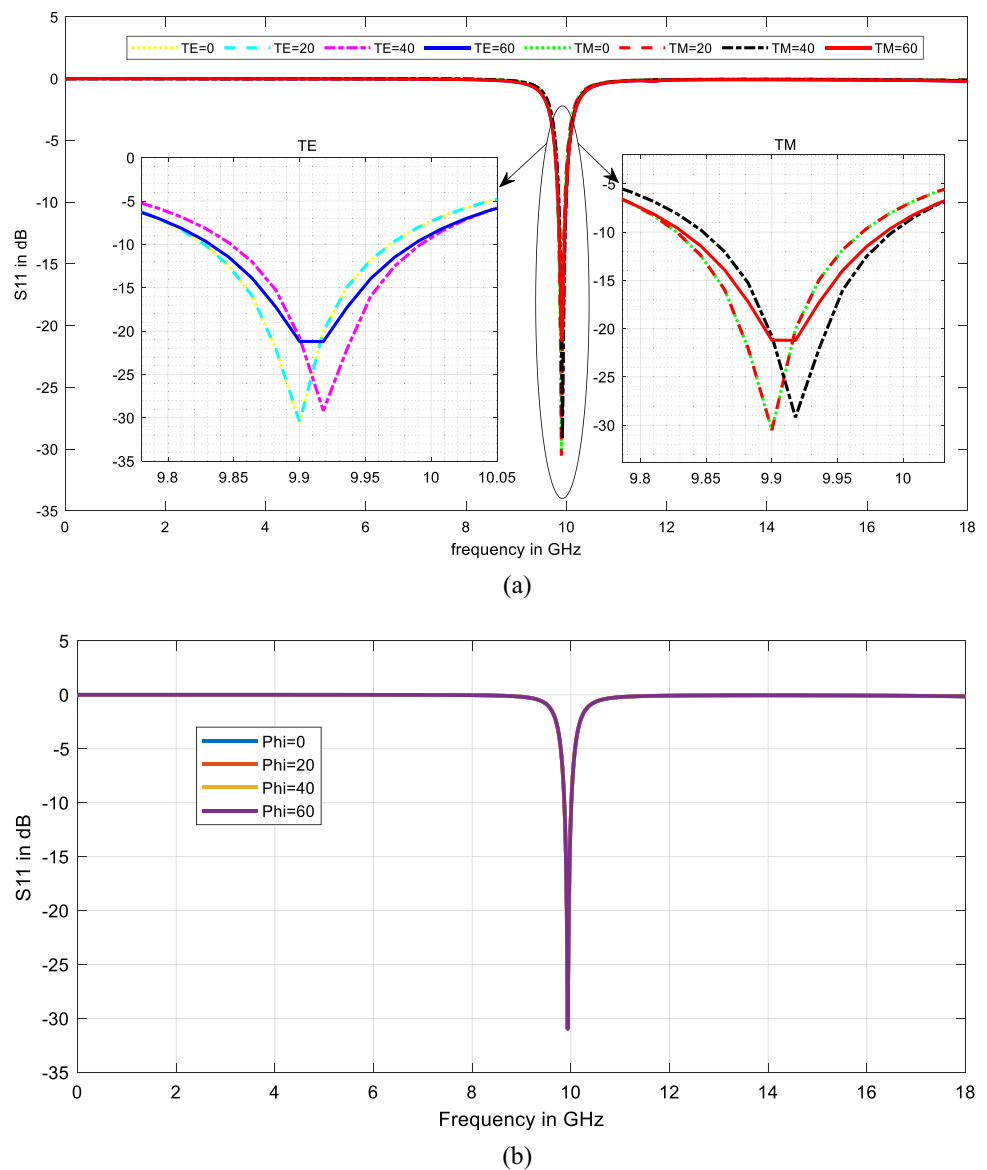
To ensure accurate and reliable results, the measurement setup was carefully calibrated using a set of calibration standards [23]. These standards are used to remove the effects of any systematic errors introduced by the measurement setup itself. The calibration procedure was performed immediately prior to the metamaterial measurements to

ensure optimal performance of the setup. In addition, the far-field distance between the metamaterial structure and the horn antenna was carefully chosen to ensure that the measurements were taken in the far-field region, where the radiation pattern of the antenna is well-defined and the field is approximately uniform. This helps to ensure that the measured reflection coefficient accurately reflects the absorptive behavior of the metamaterial structure itself, rather than being influenced by the near-field effects or other artifacts.

During the measurement process, the horn antenna was positioned normal to the surface of the metamaterial absorber, and the reflection coefficient was recorded for each frequency point in the 0–18 GHz range. The measured data were then compared with the simulated results obtained from the CST Microwave Studio simulation to validate the performance of the fabricated metamaterial absorber.

Real-time continuous measurement was carried out during the experiments, and the reflection coefficient of the metamaterial absorber was recorded and analyzed using the VNA. The simulated and measured reflection coefficient graphs of the recommended design are shown in Fig. 6c. It can be observed that the simulated peak reflection coefficient value is -30.5 dB at 9.9 GHz , whereas the measured results show that the minimum reflection coefficient value at 9.7 GHz is -28.61 dB . The simulated and measured results are hardly different, which could be owing to finite sample size and manufacturing limitations. It is worth noting that the complexity of the metamaterial structure and the surrounding environment can cause the emergence of extra peaks in the measurement. These small peaks occur due to the interplay between the metamaterial structure and the surrounding objects or measurement equipment. However, our

Fig. 5 Study the effect of distinct angles of incidence under a TE and TM (b) different polarization angles



study primarily focused on the main resonant peak of the metamaterial structure, as it is the key feature responsible for absorption. The additional peaks were not significant enough to contribute to the absorption resonance and were, therefore, ignored.

3 Sensor analysis

The MM absorber-based sensing is a potential method for distant sensing that does not require electrical contact to construct a non-invasive sensor. The reflected waves from the absorber surface are used as sensing parameters in this approach, which is not directly coupled to the spectrum analyzer. As a result, keeping the signal analyzer away from the sensors, it may make wireless sensing easier. In agriculture,

the most significant element in determining the ideal time to harvest and the greatest circumstances for safe storage is moisture content. In addition, continuous and precise monitoring of soil water content is a critical and essential metric in cultivation. The designed absorber properties that have been proposed are being examined for moisture-sensing applications in this section.

The effectiveness of any sensor is generally expressed in three characteristics. The first and foremost is that the sensor must generate a dynamic response to moisture variations. The second requirement is linearity, which means that depending on how much the measured parameter has changed, the sensor output response must vary proportionately. The last one is the sensitivity of the sensor to detect the minute change in sensing parameters. The aforementioned properties may be investigated by placing

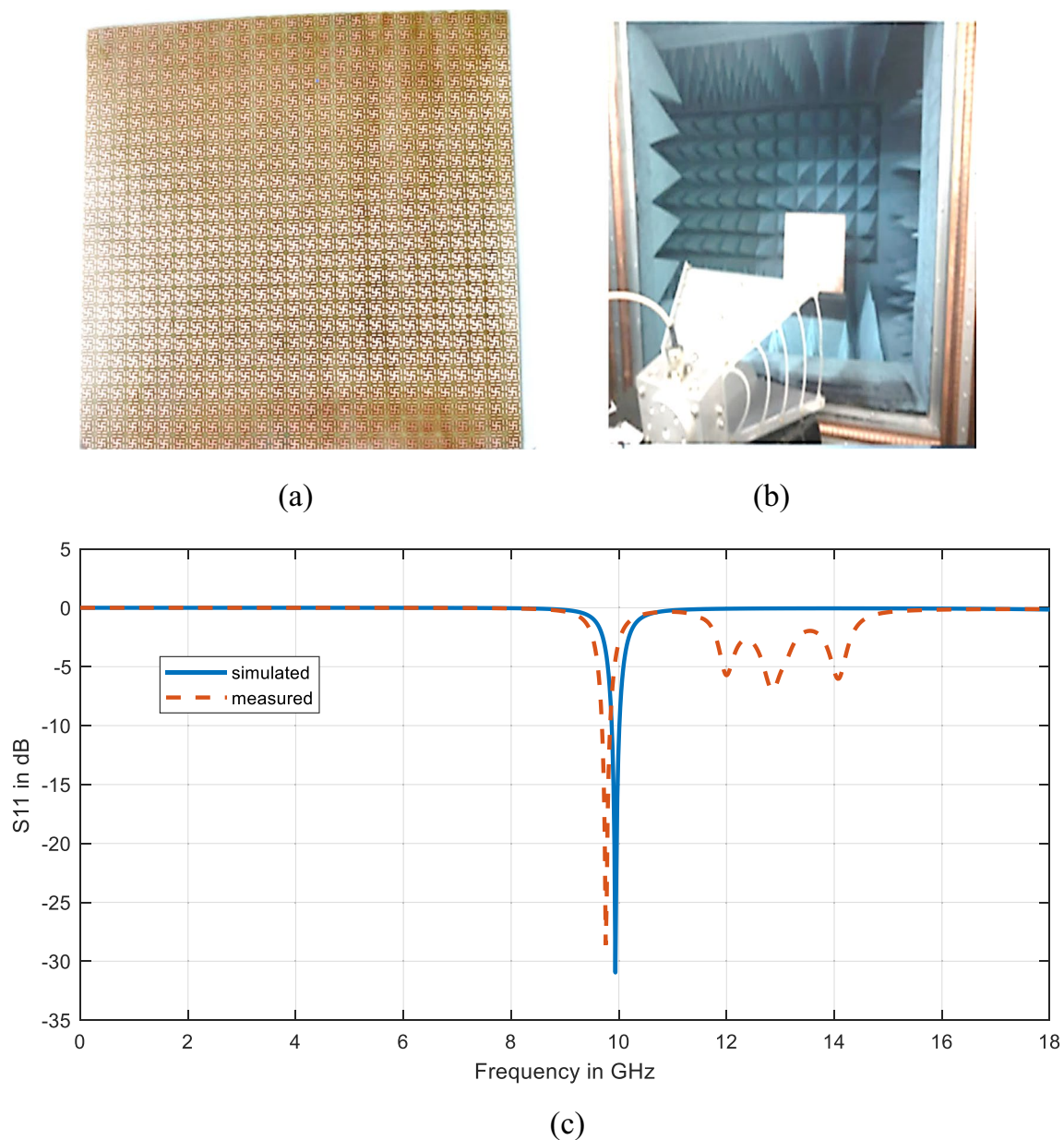


Fig. 6 **a** Front view of fabricated prototype, **b** measurement setup and **c** measured results

an analytic-sensing layer over the suggested absorber, as shown in Fig. 7. The sensing analytic layer is assumed to be made of sandy soil with different moisture contents and the corresponding permittivity and loss tangent values for the different moisture levels are estimated using [24] and are outlined in Table 2.

The sensing behavior of the suggested structure is investigated by observing the resonance frequency change with respect to moisture levels for analytic layer thickness of 0.6 mm. Figure 8 displays the absorption attained for the various volumetric moisture level with a 0.1 step shift. When the volumetric moisture level of the analytic rises,

the peak of absorption moves to the lower side of the frequency spectrum. The resonant frequency shift may be understood using the general resonance formula. Since the capacitance is proportional to sample permittivity, every increase in the sample's dielectric property increases the resonator's effective capacitance. As a result of increased capacitance, the system's resonance frequency decreases. The absorptivity attained for all of the resonance frequencies is approximately equivalent to that obtained for a perfect 100% absorption benchmark. Table 3 summarizes the results obtained for said absorber sensor.

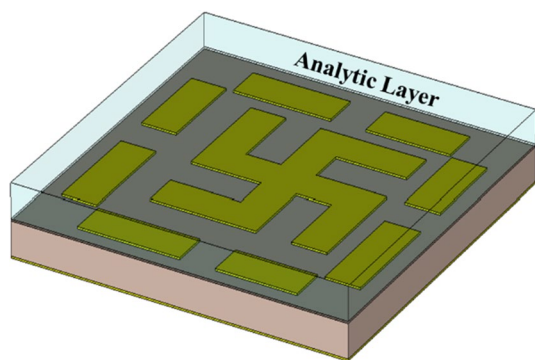


Fig. 7 Illustration of analytic layer on MM absorber

Table 2 Dielectric properties of the sandy soil for moisture levels

Permittivity	Loss tangent	Volumetric moisture
5.08	0.22	0.1
9.20	0.28	0.2
13.08	0.38	0.3
19.20	0.40	0.4
28.80	0.45	0.5

Fig. 8 Absorption of the proposed sensor for different volumetric moisture levels

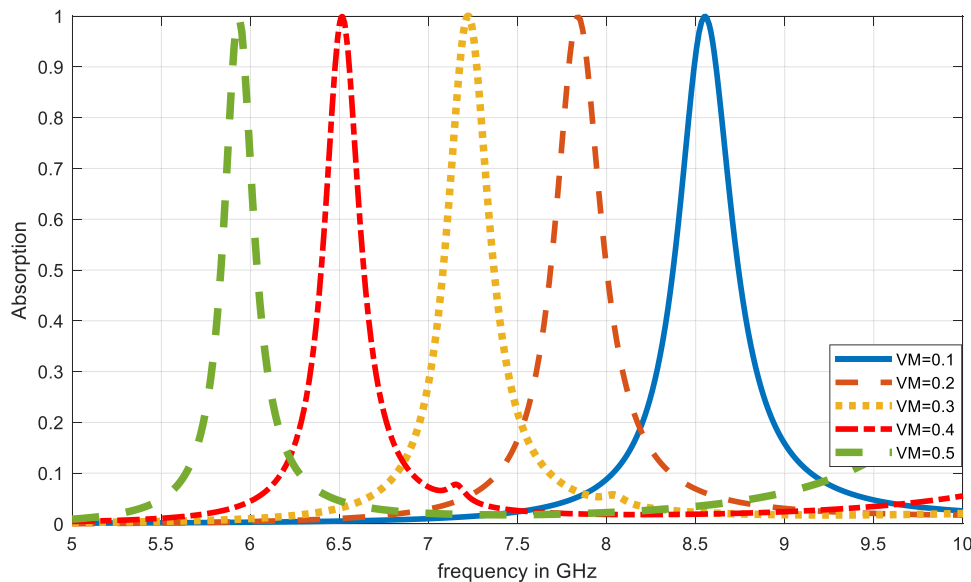


Table 3 Performance characteristics of the absorber-based moisture sensor

Volumetric moisture	Resonance peak (GHz)	Absorption (%)	FWHM (GHz)	Q factor	S (GHz/VMU)	FoM
0.1	8.55	99.92	0.2242	38.14	–	–
0.2	7.83	99.96	0.1864	42.01	7.2	38.63
0.3	7.21	99.98	0.1817	39.68	6.2	34.12
0.4	6.51	99.97	0.1391	46.8	7	50.32
0.5	5.94	99.92	0.1297	45.8	5.7	43.95

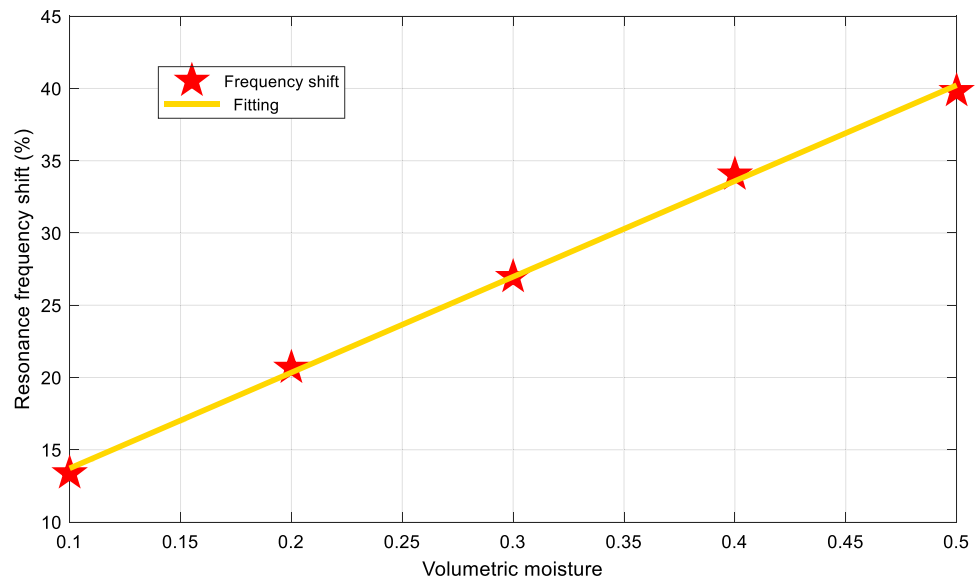
For sensing applications, excellent absorbability, high sensitivity (S), narrow bandwidth and high Quality (Q) factor is often needed. The sensitivity of this moisture sensor is determined by the relationship between the resonance frequency transition and the alteration in the volumetric moisture level. Furthermore, a single Figure of Merit (FoM) may assess all of the behavior of the sensor and is defined as the sensitivity to the Full-Width Half Maxima (FWHM) ratio. The suggested sensor’s resonant peak moves by roughly 650 MHz for a 0.1 step change in the volumetric moisture level with an FoM and aggregate sensitivity of 41.75 and 6.525 GHz/VMU, respectively.

The absorption peak shift percentage for different volumetric moisture levels is plotted in Fig. 9. Equation (1) describes quantitatively how the proposed sensor’s linearity is estimated through the curve-fitting method:

$$\Delta f(\%) = 66.27(Vm) + 7.089 \tag{1}$$

where Δf and Vm are the resonance frequency shift percentage and volumetric moisture level, respectively. The slope of the fitted curve is used to verify the sensitivity of the designed moisture sensor. In comparison with the simulated value of 6.52 GHz/VMU, the measured sensitivity of 6.62 GHz/VMU is achieved. Thus, the proposed sensor design proves to be a good candidate and shows good results

Fig. 9 Resonance frequency shift percentage with respect to volumetric moisture



in terms of resonance shift, linearity, sensitivity, *Q* factor and FoM.

The comparative analysis of the metamaterial absorbers presented in Table 4 demonstrates the exceptional performance of the current study. The absorptivity achieved in this study was 99.31%, which is higher than most of the references and is sufficient to behave as a perfect absorber. For fair comparison, the sensitivity is normalized by the absorber’s resonant frequency, and the current study outperformed most of the references. In addition, the FoM of the current study was significantly higher than the state of the art. The dimensions of the current metamaterial absorber were also relatively small and compact, making it easy to integrate into different devices.

In summary, the current study achieved outstanding results in terms of absorptivity, normalized sensitivity,

FoM, and dimensions, demonstrating the potential of the proposed metamaterial absorber for sensing applications. Furthermore, the small size and ease of fabrication of the proposed absorber make it easy to integrate into different devices, further enhancing its applicability.

4 Conclusion

An ultra-thin narrow band MM absorber is analyzed and designed in this research for moisture-sensing applications in the X band. The electromagnetic absorber consists of a 0.6 mm thick magnetic substrate sandwiched between a bottom ground layer and a top resonator layer, which work together to block incoming waves and dissipate their energy. It is observed from the simulated results that at 9.5 GHz it

Table 4 Comparison of design with state of art

Reference	Absorptivity (%)	Normalized sensitivity	FoM	Dimension
[25]	98.97	0.14	7.27	$0.36 \lambda \times 0.36 \lambda \times 0.02 \lambda$
[26]	–	0.25	4.9	$0.56 \lambda \times 0.56 \lambda \times 0.02 \lambda$
[27]	–	0.04	4.2	$1.31 \lambda \times 1.31 \lambda$
[28]	98	0.07	4.26	$0.42 \lambda \times 0.42 \lambda \times 0.16 \lambda$
[29]	99.7	0.09	6.56	$0.42 \lambda \times 0.42 \lambda \times 0.005 \lambda$
[30]	–	0.02	10.86	$0.78 \lambda \times 0.35 \lambda \times 0.05 \lambda$
[31]	99.5	0.2	5.36	$0.23 \lambda \times 0.23 \lambda \times 0.17 \lambda$
This work	99.31	0.66	41.75	$0.31 \lambda \times 0.31 \lambda \times 0.02 \lambda$

shows a -30 dB value of reflection coefficient. The simulated and measured results are well-matched with each other, which proves the usage of the proposed absorber for practical applications. With an aggregate FoM and sensitivity of 41.75 and 6.525 GHz/VMU, respectively, the suggested sensor's resonant peak moves by approximately 650 MHz for a 0.1 step change in the volumetric moisture level of the analytic test sample. The linear fitting curve's slope is used to confirm the sensitivity of the proposed moisture sensor. The measured sensitivity is 6.62 GHz/VMU, which is higher than the simulated value of 6.52 GHz/VMU. Due to its excellent qualities, the designed absorber has promising future development in the fields of moisture sensing for various agro-environmental applications.

Funding No funds, grants, or other support was received.

Availability of data and materials All data generated or analyzed during this study are included in this published article.

Declarations

Conflict of interest The authors have no conflicts of interest to declare that are relevant to the content of this article.

References

- V.G. Veselago, The electrodynamics of substrates with simultaneously negative values of ϵ and μ . *Sov. Phys. Uspekhi* **10**(4), 509–514 (1968). <https://doi.org/10.1070/PU1968v010n04ABEH003699>
- M. Amiri, F. Tofigh, N. Shariati, J. Lipman, M. Abolhasan, Review on metamaterial perfect absorbers and their applications to IoT. *IEEE Internet Things J.* **8**(6), 4105–4131 (2021). <https://doi.org/10.1109/JIOT.2020.3025585>
- M.R. Rakhshani, Narrowband plasmonic absorber using gold nanoparticle arrays for refractive index sensing. *IEEE Sens. J.* **22**(4043–4050), 1–1 (2022). <https://doi.org/10.1109/jsen.2022.3142655>
- M.Y. Azab, M.F.O. Hameed, A.M. Nasr, S.S.A. Obayya, Highly sensitive metamaterial biosensor for cancer early detection. *IEEE Sens. J.* **21**(6), 7748–7755 (2021). <https://doi.org/10.1109/JSEN.2021.3051075>
- R. Sharma, R. Khanna, G. Singla, A miniaturized highly isolated double negative metasurface MIMO antenna for sub-6GHz band. *Sadhana - Acad. Proc. Eng. Sci.* **47**(4), 1–15 (2022). <https://doi.org/10.1007/S12046-022-01987-Z/METRICS>
- H. Singh, A. Gupta, S. Bakshi, N. Mittal, Designing and analysis of non-symmetric dual layer CRLH metamaterial. *J. Magn. Mater.* **538**, 168269 (2021). <https://doi.org/10.1016/j.jmmm.2021.168269>
- N.I. Landy, S. Sajuyigbe, J.J. Mock, D.R. Smith, W.J. Padilla, Perfect metamaterial absorber. *Phys. Rev. Lett.* **100**(20), 207402 (2008). <https://doi.org/10.1103/PhysRevLett.100.207402>
- H. Singh, A. Gupta, R.S. Kaler, S. Singh, A.S. Gill, Designing and analysis of ultrathin metamaterial absorber for W band biomedical sensing application. *IEEE Sens. J.* **22**(11), 10524–10531 (2022). <https://doi.org/10.1109/jsen.2022.3168827>
- S. Ghosh, K.V. Srivastava, Polarization-insensitive single- and broadband switchable absorber/reflector and its realization using a novel biasing technique. *IEEE Trans. Antennas Propag.* **64**(8), 3665–3670 (2016). <https://doi.org/10.1109/TAP.2016.2565720>
- M.A. Al-Joumayly, N. Behdad, Low-profile, highly-selective, dual-band frequency selective surfaces with closely spaced bands of operation. *IEEE Trans. Antennas Propag.* **58**(12), 4042–4050 (2010). <https://doi.org/10.1109/TAP.2010.2078478>
- M. Sharma, N. Kumar, and R. K. Kaushal, A multiband antenna for IoT applications with two narrow-single wideband including sub-6GHz 5G NR, WLAN and UWB-X bands. *2022 2nd Int. Conf. Adv. Comput. Innov. Technol. Eng. ICACITE 2022*, pp. 499–503, 2022. <https://doi.org/10.1109/ICACITE53722.2022.9823788>
- H. Singh, B.S. Sohi, A. Gupta, Designing and analysis of cross-shaped CRLH metamaterial for wide band negative index characteristics. *Mater. Res. Express* **6**(7), 1–19 (2019). <https://doi.org/10.1088/2053-1591/ab1196>
- M. Yoo, S. Lim, Polarization-independent and ultrawideband metamaterial absorber using a hexagonal artificial impedance surface and a resistor-capacitor layer. *IEEE Trans. Antennas Propag.* **62**(5), 2652–2658 (2014). <https://doi.org/10.1109/TAP.2014.2308511>
- F. Costa, A. Monorchio, Multiband electromagnetic wave absorber based on reactive impedance ground planes. *IET Microwaves Antennas Propag.* **4**(11), 1720–1727 (2010). <https://doi.org/10.1049/IET-MAP.2009.0359/CITE/REFWORKS>
- M. Bakir, K. Delihacioglu, M. Karaaslan, F. Dincer, C. Sabah, U-shaped frequency selective surfaces for single- and dual-band applications together with absorber and sensor configurations. *IET Microwaves Antennas Propag.* **10**(3), 293–300 (2016). <https://doi.org/10.1049/IET-MAP.2015.0341>
- M. Bakir, M. Karaaslan, F. Dincer, K. Delihacioglu, C. Sabah, Tunable perfect metamaterial absorber and sensor applications. *J. Mater. Sci. Mater. Electron.* **27**(11), 12091–12099 (2016). <https://doi.org/10.1007/s10854-016-5359-7>
- D. Kundu, A. Mohan, A. Chakrabarty, Reduction of cross-polarized reflection to enhance dual-band absorption. *J. Appl. Phys.* (2016). <https://doi.org/10.1063/1.4968569>
- M. Bakir et al., Microfluidic and fuel adulteration sensing by using chiral metamaterial sensor. *J. Electrochem. Soc.* **165**(11), B475–B483 (2018). <https://doi.org/10.1149/2.0231811jes>
- R. Huang, Ultrathin metamaterial screens with nonuniform patches for reflectivity reduction from metallic surfaces. *IEEE Trans. Magn.* **49**(5), 2157–2160 (2013). <https://doi.org/10.1109/TMAG.2013.2242256>
- Y.M. Choi, J. Jung, A.S. Lee, S.S. Hwang, Photosensitive hybrid polysilsesquioxanes for etching-free processing of flexible copper clad laminate. *Compos. Sci. Technol.* **201**(November 2020), 108556 (2021). <https://doi.org/10.1016/j.compscitech.2020.108556>
- F. Urbani, Experimental analysis of novel single-sided left-handed metamaterial. *IEEE Antennas Wirel. Propag. Lett.* **9**, 720–723 (2010). <https://doi.org/10.1109/LAWP.2010.2058837>
- J. Tak, J. Choi, A wearable metamaterial microwave absorber. *IEEE Antennas Wirel. Propag. Lett.* **16**, 784–787 (2017). <https://doi.org/10.1109/LAWP.2016.2604257>
- A. Sharma, R. Panwar, R. Khanna, Experimental validation of a frequency-selective surface-loaded hybrid metamaterial absorber with wide bandwidth. *IEEE Magn. Lett.* (2019). <https://doi.org/10.1109/LMAG.2019.2898612>
- M.C. Dobson, F.T. Ulaby, M.T. Hallikainen, M.A. El-Rayes, Microwave dielectric behavior of wet soil-part II: dielectric mixing models. *IEEE Trans. Geosci. Remote Sens.* **GE-23**(1), 35–46 (1985). <https://doi.org/10.1109/TGRS.1985.289498>

25. W. Zhang, J. Li, J. Xie, R. Xu, High sensitivity refractive index sensor based on frequency selective surfaces absorber. *IEEE Sensors Lett.* **2**(3), 1–4 (2018). <https://doi.org/10.1109/lensens.2018.2862389>
26. S. Hu, S. Hu, D. Liu, D. Liu, Dual-band microwave resonators based on cross hollow structures for refractive index sensing. *Phys. Scr.* **95**(8), 1–23 (2020). <https://doi.org/10.1088/1402-4896/ab9bdd>
27. Y.I. Abdulkarim et al., The detection of chemical materials with a metamaterial-based sensor incorporating oval wing resonators. *Electron* (2020). <https://doi.org/10.3390/electronics9050825>
28. Z. Li et al., Three-band perfect absorber with high refractive index sensing based on an active tunable Dirac semimetal. *Phys. Chem. Chem. Phys.* **23**(32), 17374–17381 (2021). <https://doi.org/10.1039/d1cp01375k>
29. H. Zhu et al., A high Q-factor metamaterial absorber and its refractive index sensing characteristics. *IEEE Trans. Microw. Theory Tech.* (2022). <https://doi.org/10.1109/tmtt.2022.3218041>
30. M. Rashedul-Islam et al., Star enclosed circle split ring resonator-based metamaterial sensor for fuel and oil adulteration detection. *Alexandria Eng. J.* **67**, 547–563 (2023). <https://doi.org/10.1016/j.aej.2023.01.001>
31. M.R. Nickpay, M. Danaie, A. Shahzadi, Graphene-based tunable quad-band fan-shaped split-ring metamaterial absorber and refractive index sensor for THz spectrum. *Micro Nanostruct.* **173**, 1–8 (2023). <https://doi.org/10.1016/j.micrna.2022.207473>

Publisher's Note Springer Nature remains neutral with regard to jurisdictional claims in published maps and institutional affiliations.

Springer Nature or its licensor (e.g. a society or other partner) holds exclusive rights to this article under a publishing agreement with the author(s) or other rightsholder(s); author self-archiving of the accepted manuscript version of this article is solely governed by the terms of such publishing agreement and applicable law.